JACS
JOURNAL OF THE AMERICAN CHEMICAL SOCIETY

Article

The Soft Molecular Polycrystalline Ferroelectric Realized by Fluorination Effect

Yongfa Xie, Yong Ai, Yu-Ling Zeng, Wen-Hui He, Xue-Qin Huang, Da-Wei Fu, Ji-Xing Gao, Xiao-Gang Chen, and Yuan-Yuan Tang

J. Am. Chem. Soc., **Just Accepted Manuscript** • DOI: 10.1021/jacs.0c05372 • Publication Date (Web): 22 Jun 2020

The Soft Molecular Polycrystalline Ferroelectric Realized by Fluorination Effect

Yongfa Xie,[†] Yong Ai,[†] Yu-Ling Zeng,[†] Wen-Hui He,[†] Xue-Qin Huang,[†] Da-Wei Fu,[*,‡] Ji-Xing Gao,[‡] Xiao-Gang Chen,[‡] and Yuan-Yuan Tang[*,†]

[†]Ordered Matter Science Research Center, Nanchang University, Nanchang 330031, People's Republic of China

[‡]Institute for Science and Applications of Molecular Ferroelectrics, Key Laboratory of the Ministry of Education for Advanced Catalysis Materials, Zhejiang Normal University, Jinhua 321004, People's Republic of China

ABSTRACT: For a century ferroelectricity has attracted widespread interest from science and industry. Inorganic ferroelectric ceramics have dominated multibillion dollar industries of electronic ceramics, ranging from nonvolatile memories to piezoelectric sonar or ultrasonic transducers, whose polarization can be reoriented in multiple directions so that they can be used in the ceramic and thin film forms. However, the realization of macroscopic ferroelectricity in the polycrystalline form is challenging for molecular ferroelectrics. In pursuit of low-cost, biocompatible and mechanical flexible alternatives, the development of multiaxial molecular ferroelectrics is imminent. Here, from quinuclidinium perrhenate, we applied fluorine substitution to successfully design a multiaxial molecular ferroelectric, 3-fluoro-quinuclidinium perrhenate ([3-F-Q]ReO_4), whose macroscopic ferroelectricity can be realized in both powder compaction and thin-film forms. The fluorination effect not only increases the intrinsic polarization, but also reduces the coercive field strength. More importantly, it is also, as far as we know, the softest of all known molecular ferroelectrics, whose low Vickers hardness of 10.5 HV is comparable with that in polyvinylidene difluoride (PVDF) but almost two orders of magnitude lower than that in $BaTiO_3$. These attributes make it an ideal candidate for flexible and wearable devices, and biomechanical applications.

INTRODUCTION

Ceramics, whose history can be traced back to 27000 years ago, are inorganic, non-metallic materials shaped and subjected to heat. In addition to the importance as conventional domestic, building and art products, their unique electrical, magnetic, and optical properties also bring forth the booming of advanced ceramics in many key technologies.[1] Particularly, inorganic ferroelectric ceramics that were born in the early 1940s have been the heart and soul of several multibillion dollar industries of electronic ceramics.[2] For the usage of such inorganic materials, however, the main limitations primarily include the intrinsic brittleness and the toxicity brought by heavy metal-containing. Their processing also poses some noticeable challenges. The fabrication of inorganic ferroelectric ceramics traditionally starts with formulated oxide powders, which are then hot-pressed or sintered to the required sizes and shapes following the common sequence of mixing, drying, calcining, milling, forming, firing, and assembly.[2c] The process flow is complicated, time consuming, energy intensive, as well as necessitates high cost.[3] More than that, the high-temperature sintering or hot-pressing (even above 1000 °C for periods up to ten hours) will cause not only the loss of volatile components like Pb, Bi or Li, making it difficult to maintain the stoichiometric compositions, but also the abnormal grain growth, worsening the microstructure and thus the performance for ferroelectric ceramics.[4]

Molecular ferroelectrics, with the merits of mechanical flexibility, lightweight, structural tunability, ease of processing, biocompatibility, and low acoustical impedance, are known as promising complementary materials for the inorganic ferroelectric ceramics.[5] The past decade has witnessed the renew of research interest on new molecular ferroelectrics.[6] Some of them were found to catch up with the commercial inorganic ones such as $BaTiO_3$ in terms of the spontaneous polarization (P_s), Curie temperature (T_c), piezoelectric coefficient (d_{33}) or the number of equivalent polarization directions. A major superiority of inorganic ferroelectrics is that they can be used in polycrystalline form after poling. When a strong external electric field (10–100 kV cm^{-1}), often in combination with elevated temperature, is applied to orient the randomly distributed dipoles or domains, these polycrystalline ferroelectric materials will be able to possess both ferroelectric and piezoelectric properties, and act very similar to a single crystal. The practical use of inorganic ceramic ferroelectrics has been close to 80 years. Nevertheless, with respect to molecular ferroelectrics, the macroscopic ferroelectricity in cold-pressing polycrystalline form is still in the initial stage of exploration.[7]

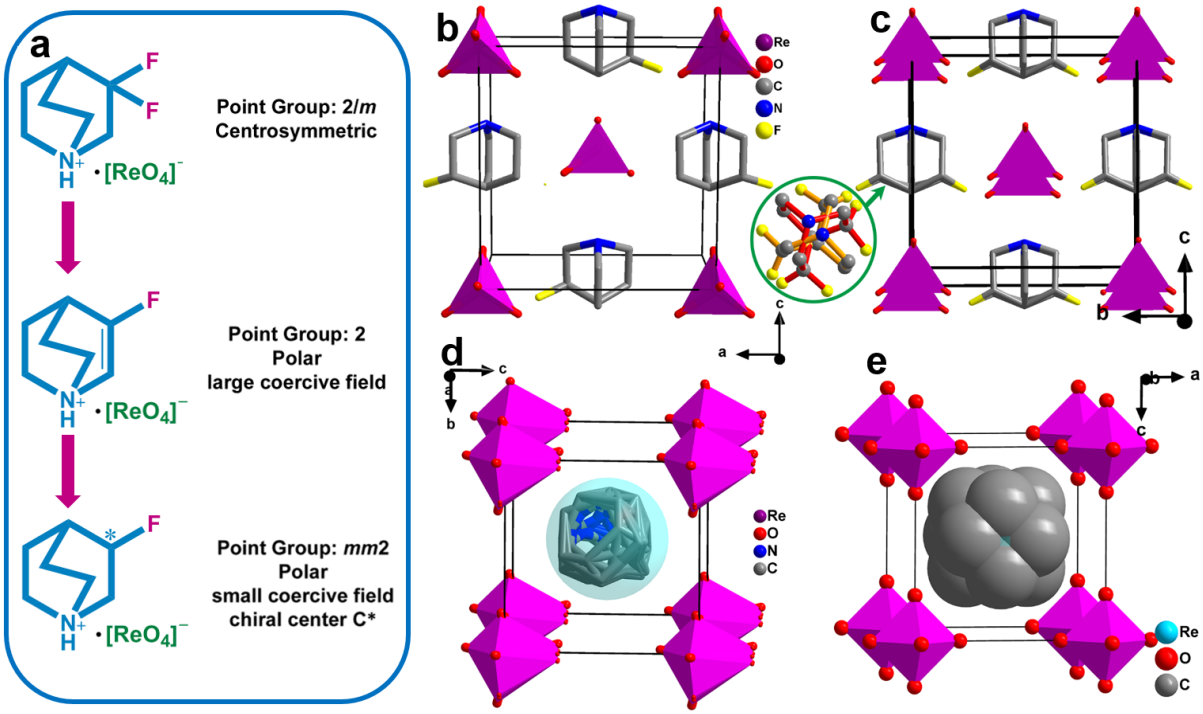

Figure 1. Molecular design strategy and crystal packing diagrams in different phases for [3-F-Q]ReO_4. (a) Molecular Design steps for [3-F-Q]ReO_4. (b) The crystal structure in the ferroelectric phase of $Pmn2_1$ at 93 K. The F atom of the 3-F-quinuclinium cation is disordered over the six possible positions, giving the *S*- or *R*-configuration, respectively. Only one distribution is illustrated for clarity. (c) The crystal structure in the ferroelectric phase of *Amm*2 at 298 K. The 3-F-quinuclinium cation is disordered over two possible positions. The F atom is disordered as the same as in the phase at 93 K. (d) The crystal structure in the ferroelectric phase of *R*3*m* at 343 K. The 3-F-quinuclinium cation is disordered around the 3-fold axis. The molecular 3-fold axis is not superimposed with the crystallographic 3-fold axis. The F atom is disordered, and not modeled. The $[ReO_4]^-$ anion is also disordered around the 3-fold axis, and the molecular 3-fold axis coincides with the crystallographic 3-fold axis. (e) The crystal structure in the paraelectric phase of $Pm\bar{3}m$ at 393 K. The organic cation is totally disordered, and modeled as a ball. The $[ReO_4]^-$ anion is also totally disordered, and modeled as an octahedron.

In contrast to the rigid inorganic systems in which the basic properties are always modified and improved by using dopants or other special chemical constituents, molecular ferroelectrics leave ample room for tuning functionalities through molecular design. We introduced an F atom to the organic cation in quinuclidinium perrhenate ([Q]ReO_4) by chemical synthesis strategy systematically (see Figures 1, S1-4 and experimental part for details), and then the single crystals of 3-fluoro-quinuclidinium perrhenate ([3-F-Q]ReO_4) were obtained by slow evaporation of room-temperature solution.[7a] Owing to the close van der Waal's radii and the similar steric parameters between H and F atoms, this new compound maintains the polar crystal structures and ferroelectric property. And, such incorporation of the most electronegative species also raised the strength of molecular dipole moment and the dynamic structural disorder might make the polarization switching easier. Moreover, [3-F-Q]ReO_4 also has low Vickers hardness of 10.5 HV comparable to that in PVDF, allowing that the powder of [3-F-Q]ReO_4 could be easily compressed into dense compaction with moderate pressure. The all room-temperature fabrication process not only reduces the cost, but also avoids any fracture during high-temperature annealing and broadens the application potential. Since there is no risk of mechanic crack-down during cooling process, customized shape would be possible using die-cast technique. As a result, it is particularly exciting to note that, single-crystal-level ferroelectric performance was successfully recorded on a fine-grained compaction pellet of the microcrystalline powders made by cold-pressing at room temperature. This discovery points out the bright future of molecular ferroelectrics in the polycrystalline form, while the simple room-temperature processing without sintering or hot-pressing will be a deciding factor in the design of flexible and wearable electronic devices.

RESULTS AND DISCUSSION

The synthetic strategy was shown in Figure 1a, which started with quinuclidin-3-one. All three fluorine-containing products react with perrhenic acid to verify their potential ferroelectricity. The first obtained fluorine-containing product is 3,3-difluoroquinuclidine. Its perrhenate salt crystallizes in centrosymmetric point group 2/*m*. Under the influence of fluorination, the symmetry of [3,3-difluoro-quinuclidinium]ReO_4 is lowered compared with [Q]ReO_4 crystal, but the anti-parallel 3,3-difluoro-quinuclidinium cations lead to the centrosymmetric packing of crystal (Figure S1).[7a] Thus no ferroelectricity can be expected. The second fluorine-

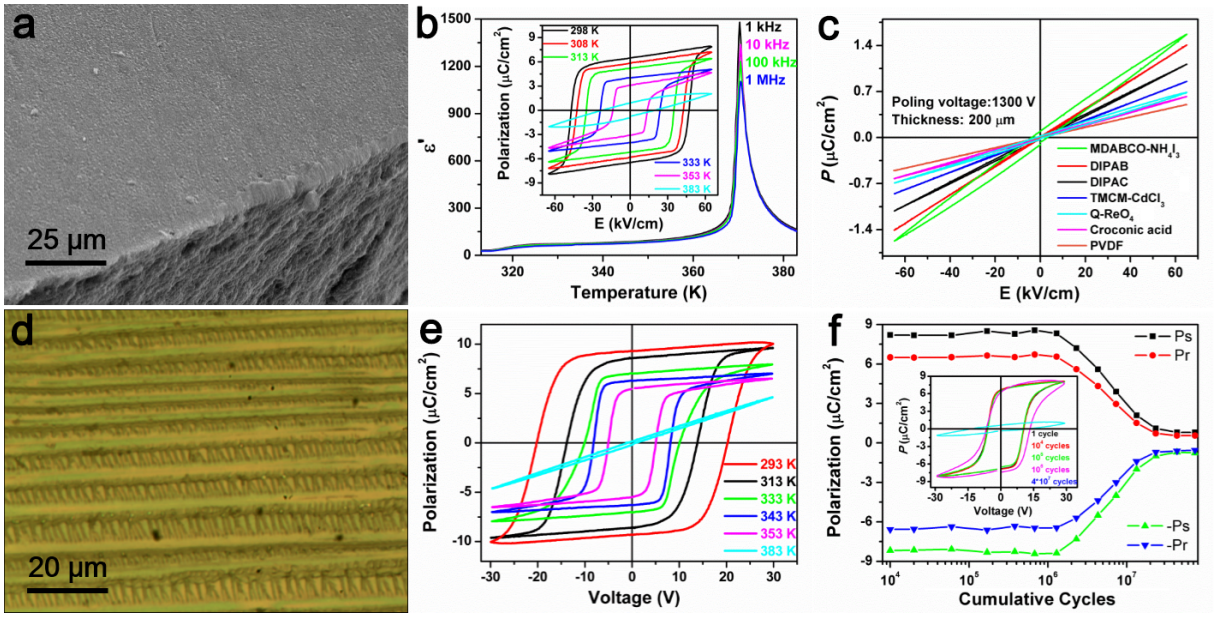

Figure 2. Ferroelectric properties of [3-F-Q]ReO_4. (a) SEM image of the powder compaction. (b) Temperature dependence of dielectric constant at different frequencies. The insert shows the *P–E* hysteresis loops obtained on the powder compaction sample at different temperatures. (c) Linear *P–E* relationship of some typical molecular ferroelectrics with the powder compaction form under the same electric field. (d) Optical microscope photograph of thin film. (e) *P–E* hysteresis loops measured on the thin film sample under different temperatures at 1 kHz. (f) Fatigue characteristics of the ferroelectric thin film at room temperature, and the inset shows the *P–E* relationship after different switching cycles.

containing product is 3-fluoro-1-azabicyclo[2.2.2]oct-2-ene. The carbon atom at the 3 position is changed from sp^3 hybridization to sp^2 hybridization. The fluorination effect also lowers the symmetry of crystal, and it crystallizes in a polar point group 2. The potential ferroelectricity is examined by PFM domain mapping and switching spectroscopy (Figures S2-4), which shows the switchable polarization with relative large coercive field (about 5 times larger than that of [3-F-Q]ReO_4). The large coercive field may be due to the ordered structure stabilized by hydrogen bonding effect. Finally, 3-fluoroquinuclidine was obtained by catalytic hydrogenation from 3-fluoro-1-azabicyclo[2.2.2]oct-2-ene. Compared with [Q]ReO_4 crystal, only one H atom is substituted by one F atom. Such subtle fluorination effect can introduce a chiral center, leading to a variety of possible molecular design results. In this case, the stoichiometric *R*- and *S*-3-fluoroquinuclidine crystallize together with perrhenic acid. The symmetry of the resultant crystal maintains *mm*2 point group, which is the same of [Q]ReO_4 crystal. Therefore, the advantages of fluorination can be summarized as follows: (1) The inherent C–F dipole could enhance the ferroelectric polarization essentially; (2) It is possible to regulate the polarization direction or equivalent number of polarization directions since the crystal symmetry can be maintained or lowered due to fluorination effect; (3) Chiral centers could be introduced by fluorination, which can be used to targeted design of chiral ferroelectrics.

The [3-F-Q]ReO_4 crystal undergoes three phase transitions at around 285, 319 and 370 K, from the low-temperature phase (LTP) $Pmn2_1$, to the intermediate-temperature phase (ITP1) *Amm*2, to the intermediate-temperature phase (ITP2) *R*3*m*, and to the high-temperature phase (HTP) $Pm\bar{3}m$ (Figures 1 and S5). Also, temperature-dependent second harmonic generation measurement shows the structural symmetry variation from centrosymmetric paraelectric phase to non-centrosymmetric ferroelectric phases (Figure S6). The crystal structure is similar to that of non-fluorine-substituted specimen,[7a] which adopts the simple cubic structure in the paraelectric phase, where the $[ReO_4]^-$ anions occupy the vertexes of cubic cell, and the 3-F-quinuclinium cation occupies the center (Figure 1e). The structural differences for different phases are mainly in the orientation states of the isolated cations and anions. The substitution of an F atom for an H atom does not affect the structures significantly, and accordingly the crystal symmetry for three of the four phases is the same as that for non-fluorine-substituted specimen, whereas a new phase of *Amm*2 is observed. The polarization direction of $Pmn2_1$ and *Amm*2 phases is confined to [110]-direction with regard to the high-temperature cubic $Pm\bar{3}m$ phase, which has 12 equivalent polarization directions. While the polarization direction of the *R*3*m* phase is along the [111]-direction, which has 8 equivalent directions. For three crystals, the packing structures are very similar, while the anti-parallel 3,3-difluoro-quinuclidinium cations lead to the centrosymmetric structure and the parallel 3-fluoro-1-azabicyclo[2.2.2]oct-2-ene and 3-F-quinuclidinium cations result in the polar structure with the ferroelectric spontaneous polarization (Figure S7).

The macroscopic ferroelectricity of [3-F-Q]ReO_4 was first examined by the powder compression form. [3-F-Q]ReO_4 can exhibit impressive mechanical properties, where the Vickers hardness of 10.5 HV was obtained on single crystalline sample. We measured the Vickers

hardness of several representative ferroelectrics with the same nanoindenter and compared their values as listed in Table S1. [3-F-Q]ReO_4 possesses the smallest Vickers hardness among molecular ferroelectrics, which is comparable with ferroelectric polymer PVDF. Hence, the powder could be easily compressed into dense compaction disc with moderate pressure at room temperature. In Figure 2a, scanning electron microscope (SEM) image shows that a dense pore-less powder compaction, which is similar to the ceramic-form of inorganic ferroelectrics. Then, the polarization vs. electric field (*P–E*) hysteresis loops of such powder compaction are measured. As shown in Figure 2b, by applying a 50 Hz AC voltage, well-defined rectangular *P–E* hysteresis loops can be obtained at different temperatures, which undoubtedly confirm the ferroelectricity in the powder compaction form. The remanent polarization (P_r) is extracted with zero electric field of P_r = 6.0 μC cm^{-2} at room temperature. The fact that the P_r is smaller than the theoretical value is possibly due to the randomly oriented polycrystalline grains in the powder sample.[8] For the powder compaction form, as increasing temperature from 298 to 313 K, the P_r decreases slightly, which is most likely caused by the increase of thermal fluctuation that disrupts the long-range order of polarization upon heating. From 313 K to 333 K, the drop of remanent polarization is more prominent, which can be attributed to the orthorhombic-to-trigonal phase transition at 319 K. Moreover, the coercive field (E_c) shows a decrease with increasing temperature, which should be attributed to the weakening of the coupling stabilizing effect between the domains.[9] For comparison, the ferroelectricity of some typical molecular ferroelectrics (MDABCO-NH_4I_3,[6a] DIPAB,[6b] DIPAC,[10] TMCM-$CdCl_3$,[6c] [Q]ReO_4,[7a] croconic acid,[11] and PVDF) with powder compaction form are examined under the same condition at room temperature (Figure 2c). Under the maximum electric field 65 kV/cm, only linear *P–E* relationship are observed, indicating that the dipoles are hard to be switched in the polycrystalline form. Therein, the relative large coercive field and mono-axis character might be two main factors for the unswitchable ferroelectricity in the powder compaction form.

Along with the rapid development of integrated electronic application, the predominance of molecular ferroelectrics that can be easily fabricated by low-temperature and cost-saving solution method thin films becomes more and more obvious. As seen from Figure 2d, the as-prepared thin-film of [3-F-Q]ReO_4 shows large area with high coverage. The ferroelectric performance of the thin film was tested with AC frequency of 1 kHz, in the temperature range of 293 to 353 K. The obtained *P–E* hysteresis loops always retain good rectangularity (Figure 2e), which discloses the robust ferroelectricity of the [3-F-Q]ReO_4 thin film in a wide temperature range and thus the suitability for high-temperature working environment. The P_r values remain 8 to 5 μC cm^{-2}, close to that of the theoretical value. Notably, the polarization switching speed (1 kHz) is fast among molecular ferroelectrics, which provides [3-F-Q]ReO_4 more practical potential in electronic applications. Moreover, the remanent polarization of thin film can be maintained till 10^6 cycles without any deterioration (Figure 2f), shows excellent fatigue properties.

Using piezoresponse force microscopy (PFM), we observed the stable and switchable polarization in the [3-F-Q]ReO_4 film, which is the most intrinsic property of ferroelectrics (Figure 3).[12] Because of the presence of stress imposed by the matrix, the as-grown film surface exhibits various domain patterns at room temperature in the ITP1 (Figure S8), including the intriguing herringbone multidomain structure (Figure 3a). As shown in Figure S8b, the striking 180° contrasts both in the out-of-plane and in-plane phase images indicate that the polarizations are antiparallel in two adjacent domains. Meanwhile, in the amplitude images, the signal is necessarily nulling at domain walls and nearly equal in adjacent domains, suggesting they are 180° domain walls. In contrast, Figure S8c exhibits inconsistent phase contrasts and various amplitude signals in adjacent domains, where these domain walls should be non-180° ones. Through comprehensive PFM studies, we clearly identified the coexistence of 180° and non-180° ferroelectric domains, confirming the multiaxial nature in [3-F-Q]ReO_4.

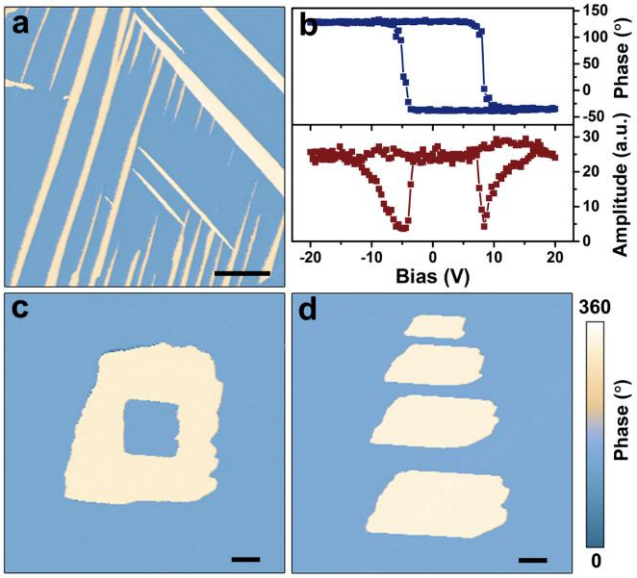

Figure 3. Microscopic ferroelectric properties of [3-F-Q]ReO_4 at room temperature in the ITP1. (a) Out-of-plane PFM phase image in the film, showing the beautiful herringbone ferroelectric domain structure. (b) Hysteretic dependence of out-of-plane PFM phase and amplitude with applied DC bias for the film. (c) Out-of-plane phase image for 0.6 μm thick film with written box-in-box patterns under reversed DC bias ±12 V. (d) Out-of-plane phase image of domains written by +15 V bias pulses of various durations 0.3 s, 0.6 s, 0.9 s and 1.2 s in a 0.6 μm thick film. Scale bars: 2 μm.

To characterize the switching behavior, we performed local PFM-based hysteresis loop measurements and local polarization manipulation experiments in the [3-F-Q]ReO_4 films with different thicknesses (Figures 3 and S9-11). The characteristic hysteresis and butterfly loops constitute a proof of the switching of ferroelectric domains. By

averaging the minima of the amplitude hysteresis loops, we can estimate that local coercive voltages (V_c) of 1.5, 1 and 0.6 μm thick films are 15.5, 9 and 6.6 V, respectively (Figures S9a-c). Such low operating voltages will be desirable for memory devices. Figures S9d-f demonstrate the out-of-plane phase images of 1.5, 1 and 0.6 μm thick films after writing box-in-box patterns with reversed DC bias in the centre. The large phase contrast (~180°) can be observed, suggesting that opposite polarizations have been written in the [3-F-Q]ReO_4 film. The switching voltage in a film with thickness about 1.5 μm is only 20 V, much smaller than 100 V in the [3-F-Q]ReO_4 film with the same thickness.[13] Figures 3d and S11 present the poling map acquired by applying a constant DC bias of +15 V to the tip with a pulse duration ranging from 0.3 to 1.2 s for a 0.6 μm thick film, where the written domains vary markedly with the change of time. All the above evidence establishes the presence of ferroelectricity in the [3-F-Q]ReO_4 film.

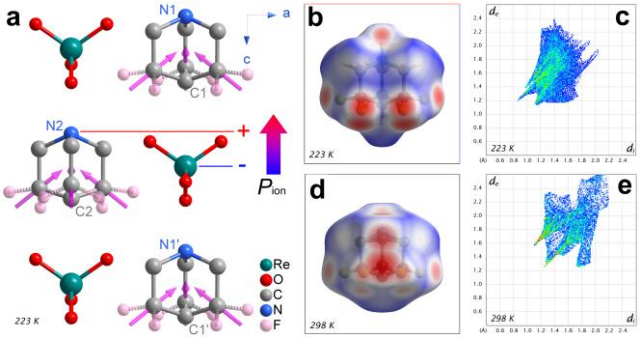

Figure 4. Ferroelectric polarization characteristics of [3-F-Q]ReO_4. (a) Schematic drawing of polarization along crystallographic *c*-axis originating from ionic displacement (P_{ion}) and C–F dipoles (magenta arrows). Hirshfeld surfaces (b, d) and 2D fingerprint plots (c, e) of F-quinuclidine molecule at different temperatures.

The ferroelectric polarization in [3-F-Q]ReO_4 crystal is firstly evaluated by point charge model analysis (Tables S2 and S3). The obvious displacement between positive charged $[3\text{-F-Q}]^+$ and negative $[ReO_4]^-$ gives a major source of polarization about 8.30 $\mu C/cm^2$ and 8.52 $\mu C/cm^2$ along *c* axis at 223 K and 298 K, respectively, which are obviously larger than [Q]ReO_4 crystal (7.58 $\mu C/cm^2$).[13] Secondly, to investigate the C–F dipole on the ferroelectric polarization in [3-F-Q]ReO_4 crystal, DFT calculations on the dipole moment are carried out. When the 3-H atom was substituted by F atom, the large dipole moment of C–F bond (2.09–2.34 D) would have a huge impact on the polarization value. Considering the direction of the C–F bond in [3-F-Q]ReO_4 crystal (Figure 4a), the effective contribution from polar C–F bond to the ferroelectric polarization along crystallographic *c* axis is about 1.0 $\mu C/cm^2$. Therefore, through F atom substitution, both the ionic displacement and C–F dipole can enhance the total polarization of [3-F-Q]ReO_4 crystal, which can be estimated to be 7.6 $\mu C/cm^2$. Compared with [Q]ReO_4 crystal, the polarization value increases 30% (1.72 $\mu C/cm^2$) due to the F-substitution effect. From this point of view, the well-designed F atom substitution is an effective strategy to enhance the ferroelectric polarization performance.

On the other hand, the F-quinuclidine molecules have experienced different dynamic states with increasing temperature. Intermolecular interactions between F-quinuclidine molecules and surrounding environments in this process were quantified using Hirshfeld surfaces (Figures 4b, 4d, and S12).[14] The color coding in Hirshfeld surfaces (d_{norm} mode) shows the normalized contact distance based upon the location and magnitudes of intermolecular interactions. Where atoms make intermolecular contacts closer than the sum of their van der Waals radii, these contacts will be highlighted in red on the d_{norm} surface. Longer contacts are blue, and contacts around the sum of van der Waals radii are white. At 223 K, large red areas in the Hirshfeld surface are observed from the C–F peripheries, indicating strong intermolecular interactions. Below 223 K, there is no distinct variation of the F-quinuclidine dynamic behavior, so the Hirshfeld surfaces and corresponding fingerprint plots only change slightly (Figure S12). On the other side, the F-quinuclidine structure is disordered along 2-fold rotation axis at 298 K. Consequently, the red areas in the Hirshfeld surface transferred to the side parts (Figure 4d), which means the 2-fold disorder dominates the inter-molecular interactions instead of elongate C–F group. At the same time, the decoded two-dimensional (2D) fingerprint plots shifting to the longer contact direction also indicates the relaxed inter-molecular interactions and then probably lower the coercive field for the ferroelectric switching (Figures 4c and 4e). Similarly, the short contact red areas shrink and move to the end of the body diagonal ends since the F-quinuclidine displays 3-fold disorder at 434 K (Figures S12i-j), and finally disappear at the high-degree disordered cubic states (Figures S12k-l). In the process of changing with temperature, the globularity (is a measure of the degree to which the surface area differs from the value for a sphere of the same volume) of the F-quinuclidine increases monotonically, also reflects its dynamic behavior (Figure S13). We also compared the intermolecular contacts of [3-F-Q]ReO_4 with those of [3,3-difluoro-quinuclidinium]ReO_4 and [3-fluoro-1-azabicyclo[2.2.2]oct-2-en-1-ium]ReO_4 by the 2D fingerprint plots of cations. As shown in Figures S12 and S14, the short contacts between cation and its surroundings with minimum (d_i, d_e) of (0.703, 1.060) in [3,3-difluoro-quinuclidinium]ReO_4 are much stronger than those of (0.895, 1.182) in [3-fluoro-1-azabicyclo[2.2.2]oct-2-en-1-ium]ReO_4 and (0.899, 1.158) in [3-F-Q]ReO_4. This may be one reason why its phase transition temperature (388 K) is relatively higher than theirs (366 K and 370 K).

CONCLUSION

Through elaborate fluorine atom substitution, we have found excellent ferroelectricity in a molecular ferroelectric of 3-fluoro-quinuclidinium perrhenate, which displays macroscopic ferroelectricity in both powder compaction and thin-film forms. On the one hand, the fluorination effect not only enhance the intrinsic ferroelectric

polarization without changing the symmetry of the point group of the crystal, but also lower the coercive field. On the other hand, unlike $BaTiO_3$ and other ferroelectric ceramics which need long-time high-temperature sintering, the powder compaction of [3-F-Q]ReO_4 is fabricated by simple cold-pressing method at room temperature due to the smallest Vickers hardness among molecular ferroelectrics. The room-temperature fabrication not only reduces cost, but also avoids any fracture during high-temperature annealing and broadens the application potential. Molecular ferroelectrics can be used in the cold-pressing polycrystalline form like inorganic ferroelectrics, which opens up a new path for the application of 'molecular polycrystalline ferroelectrics'. Furthermore, the thin-film of [3-F-Q]ReO_4 can be simply prepared by aqueous method, which has potential application in soft piezoelectrics, thin-film memory, flexible electronics, *etc*.

ASSOCIATED CONTENT

Supporting Information.

Sample preparation, X-ray crystallographic, differential scanning calorimetry, dielectric, SHG, PFM characterizations, computational modelling, Figures S1–S14, and Tables S1–S3. This material is available free of charge via the Internet at http://pubs.acs.org.

AUTHOR INFORMATION

Corresponding Author

*dawei@zjnu.edu.cn; tangyuanyuan@ncu.edu.cn

Notes

The authors declare no competing financial interests.

ACKNOWLEDGMENT

This work was financially supported by the National Natural Science Foundation of China (21991141, 21975114, and 11904151), the Natural Science Foundation of Zhejiang Province (LZ20B010001), and starting grants from Zhejiang Normal University.

REFERENCES

(1) (a) Saito, Y.; Takao, H.; Tani, T.; Nonoyama, T.; Takatori, K.; Homma, T.; Nagaya, T.; Nakamura, M. Lead-free piezoceramics. *Nature* **2004**, *432*, 84. (b) Pullar, R. C. Hexagonal ferrites: A review of the synthesis, properties and applications of hexaferrite ceramics. *Prog. Mater. Sci.* **2012**, *57*, 1191. (c) Minh, N. Q. Ceramic Fuel Cells. *J. Am. Ceram. Soc.* **1993**, *76*, 563.

(2) (a) Scott, J. F. Applications of modern ferroelectrics. *Science* **2007**, *315*, 954. (b) Scott, J. F.; Araujo, C. P. d. Ferroelectric memories. *Science* **1989**, *246*, 1400. (c) Haertling, G. H. Ferroelectric ceramics: history and technology. *J. Am. Ceram. Soc.* **1999**, *82*, 797. (d) Li, F.; Cabral, M. J.; Xu, B.; Cheng, Z.; Dickey, E. C.; LeBeau, J. M.; Wang, J.; Luo, J.; Taylor, S.; Hackenberger, W.; Bellaiche, L.; Xu, Z.; Chen, L.-Q.; Shrout, T. R.; Zhang, S. Giant piezoelectricity of Sm-doped $Pb(Mg_{1/3}Nb_{2/3})O_3$-$PbTiO_3$ single crystals. *Science* **2019**, *364*, 264. (e) Qiu, C.; Wang, B.; Zhang, N.; Zhang, S.; Liu, J.; Walker, D.; Wang, Y.; Tian, H.; Shrout, T. R.; Xu, Z. Transparent ferroelectric crystals with ultrahigh piezoelectricity. *Nature* **2020**, *577*, 350. (f) Zhang, L.; Chen, J.; Fan, L.; Diéguez, O.; Cao, J.; Pan, Z.; Wang, Y.; Wang, J.; Kim, M.; Deng, S.; Wang, J.; Wang, H.; Deng, J.; Yu, R.; Scott, J. F.; Xing, X. Giant polarization in super-tetragonal thin films through interphase strain. *Science* **2018**, *361*, 494.

(3) Ramadan, K. S.; Sameoto, D.; Evoy, S. A review of piezoelectric polymers as functional materials for electromechanical transducers. *Smart Mater. Struct.* **2014**, *23*, 33001.

(4) Kong, L. B.; Zhang, T. S.; Ma, J.; Boey, F. Progress in synthesis of ferroelectric ceramic materials via high-energy mechanochemical technique. *Prog. Mater Sci.* **2008**, *53*, 207.

(5) (a) Li, W.; Wang, Z.; Deschler, F.; Gao, S.; Friend, R. H.; Cheetham, A. K. Chemically diverse and multifunctional hybrid organic–inorganic perovskites. *Nat. Rev. Mater.* **2017**, *2*, 16099. (b) Xu, W.-J.; Li, P.-F.; Tang, Y.-Y.; Zhang, W.-X.; Xiong, R.-G.; Chen, X.-M. A Molecular Perovskite with Switchable Coordination Bonds for High-Temperature Multiaxial Ferroelectrics. *J. Am. Chem. Soc.* **2017**, *139*, 6369. (c) Zhang, Z.; Li, P.-F.; Tang, Y.-Y.; Wilson, A. J.; Willets, K.; Wuttig, M.; Xiong, R.-G.; Ren, S. Tunable electroresistance and electro-optic effects of transparent molecular ferroelectrics. *Sci. Adv.* **2017**, *3*, e1701008. (d) Gao, W.; Zhang, Z.; Li, P. F.; Tang, Y. Y.; Xiong, R. G.; Yuan, G.; Ren, S. Chiral Molecular Ferroelectrics with Polarized Optical Effect and Electroresistive Switching. *ACS Nano* **2017**, *11*, 11739. (e) Li, D.; Zhao, X.-M.; Zhao, H.-X.; Dong, X.-W.; Long, L.-S.; Zheng, L.-S. Construction of Magnetoelectric Composites with a Large Room-Temperature Magnetoelectric Response through Molecular–Ionic Ferroelectrics. *Adv. Mater.* **2018**, *30*, 1803716. (f) Zhang, H.-Y.; Song, X.-J.; Chen, X.-G.; Zhang, Z.-X.; You, Y.-M.; Tang, Y.-Y.; Xiong, R.-G. Observation of Vortex Domains in a Two-Dimensional Lead Iodide Perovskite Ferroelectric. *J. Am. Chem. Soc.* **2020**, *142*, 4925.

(6) (a) Ye, H. Y.; Tang, Y. Y.; Li, P. F.; Liao, W. Q.; Gao, J. X.; Hua, X. N.; Cai, H.; Shi, P. P.; You, Y. M.; Xiong, R. G. Metal-free three-dimensional perovskite ferroelectrics. *Science* **2018**, *361*, 151. (b) Fu, D. W.; Cai, H. L.; Liu, Y. M.; Ye, Q.; Zhang, W.; Zhang, Y.; Chen, X. Y.; Giovannetti, G.; Capone, M.; Li, J. Y.; Xiong, R. G. Diisopropylammonium Bromide Is a High-Temperature Molecular Ferroelectric Crystal. *Science* **2013**, *339*, 425. (c) You, Y. M.; Liao, W. Q.; Zhao, D. W.; Ye, H. Y.; Zhang, Y.; Zhou, Q. H.; Niu, X. H.; Wang, J. L.; Li, P. F.; Fu, D. W.; Wang, Z. M.; Gao, S.; Yang, K. L.; Liu, J. M.; Li, J. Y.; Yan, Y. F.; Xiong, R. G. An organic-inorganic perovskite ferroelectric with large piezoelectric response. *Science* **2017**, *357*, 306. (d) Liao, W. Q.; Zhao, D. W.; Tang, Y. Y.; Zhang, Y.; Li, P. F.; Shi, P. P.; Chen, X. G.; You, Y. M.; Xiong, R. G. A molecular perovskite solid solution with piezoelectricity stronger than lead zirconate titanate. *Science* **2019**, *363*, 1206. (e) Anetai, H.; Takeda, T.; Hoshino, N.; Kobayashi, H.; Saito, N.; Shigeno, M.; Yamaguchi, M.; Akutagawa, T. Ferroelectric Alkylamide-Substituted Helicene Derivative with Two-Dimensional Hydrogen-Bonding Lamellar Phase. *J. Am. Chem. Soc.* **2019**, *141*, 2391. (f) Li, P.-F.; Liao, W.-Q.; Tang, Y.-Y.; Qiao, W.; Zhao, D.; Ai, Y.; Yao, Y.-F.; Xiong, R.-G. Organic enantiomeric high-T_c ferroelectrics. *Proc. Natl. Acad. Sci. U. S. A.* **2019**, *116*, 5878. (g) Han, S.; Liu, X.; Liu, Y.; Xu, Z.; Li, Y.; Hong, M.; Luo, J.; Sun, Z. High-Temperature Antiferroelectric of Lead Iodide Hybrid Perovskites. *J. Am. Chem. Soc.* **2019**, *141*, 12470. (h) Li, L.; Liu, X.; Li, Y.; Xu, Z.; Wu, Z.; Han, S.; Tao, K.; Hong, M.; Luo, J.; Sun, Z. Two-Dimensional Hybrid Perovskite-Type Ferroelectric for Highly Polarization-Sensitive Shortwave Photodetection. *J. Am. Chem. Soc.* **2019**, *141*, 2623. (i) Tang, Y.-Y.; Ai, Y.; Liao, W.-Q.; Li, P.-F.; Wang, Z.-X.; Xiong, R.-G. H/F-Substitution-Induced Homochirality for Designing High-T_c Molecular Perovskite Ferroelectrics. *Adv. Mater.* **2019**, *31*, 1902163. (j) Yao, Z. S.; Yamamoto, K.; Cai, H. L.; Takahashi, K.; Sato, O. Above Room Temperature Organic Ferroelectrics: Diprotonated 1,4-Diazabicyclo[2.2.2]octane Shifts between Two 2-Chlorobenzoates. *J. Am. Chem. Soc.* **2016**, *138*, 12005. (k) Chen, L.; Liao, W.-Q.; Ai, Y.; Li, J.; Deng, S.; Hou, Y.; Tang, Y.-Y. Precise Molecular Design Toward Organic–Inorganic Zinc Chloride ABX_3 Ferroelectrics. *J. Am. Chem. Soc.* **2020**, *142*, 6236.

(7) (a) Harada, J.; Shimojo, T.; Oyamaguchi, H.; Hasegawa, H.; Takahashi, Y.; Satomi, K.; Suzuki, Y.; Kawamata, J.; Inabe, T. Directionally tunable and mechanically deformable ferroelectric crystals from rotating polar globular ionic molecules. *Nat. Chem.* **2016**, *8*, 946. (b) Harada, J.; Yoneyama, N.; Yokokura, S.; Takahashi, Y.; Miura, A.; Kitamura, N.; Inabe, T. Ferroelectricity and Piezoelectricity in Free-Standing Polycrystalline Films of Plastic Crystals. *J. Am. Chem. Soc.* **2018**, *140*, 346. (c) Tang, Y. Y.; Li, P. F.; Liao, W. Q.; Shi, P. P.; You, Y. M.; Xiong, R. G. Multiaxial Molecular Ferroelectric Thin Films Bring Light to Practical Applications. *J. Am. Chem. Soc.* **2018**, *140*, 8051.

(8) Damjanovic, D. Ferroelectric, dielectric and piezoelectric properties of ferroelectric thin films and ceramics. *Rep. Prog. Phys.* **1998**, *61*, 1267.

(9) Jin, L.; Li, F.; Zhang, S.; Green, D. J. Decoding the Fingerprint of Ferroelectric Loops: Comprehension of the Material Properties and Structures. *J. Am. Ceram. Soc.* **2014**, *97*, 1.

(10) Fu, D. W.; Zhang, W.; Cai, H. L.; Ge, J. Z.; Zhang, Y.; Xiong, R. G. Diisopropylammonium Chloride: A Ferroelectric Organic Salt with a High Phase Transition Temperature and Practical Utilization Level of Spontaneous Polarization. *Adv. Mater.* **2011**, *23*, 5658.

(11) Horiuchi, S.; Tokunaga, Y.; Giovannetti, G.; Picozzi, S.; Itoh, H.; Shimano, R.; Kumai, R.; Tokura, Y. Above-room-temperature ferroelectricity in a single-component molecular crystal. *Nature* **2010**, *463*, 789.

(12) (a) Garcia, V.; Fusil, S.; Bouzehouane, K.; Enouz-Vedrenne, S.; Mathur, N. D.; Barthelemy, A.; Bibes, M. Giant tunnel electroresistance for non-destructive readout of ferroelectric states. *Nature* **2009**, *460*, 81. (b) Lee, D.; Lu, H.; Gu, Y.; Choi, S.-Y.; Li, S.-D.; Ryu, S.; Paudel, T. R.; Song, K.; Mikheev, E.; Lee, S.; Stemmer, S.; Tenne, D. A.; Oh, S. H.; Tsymbal, E. Y.; Wu, X.; Chen, L.-Q.; Gruverman, A.; Eom, C. B. Emergence of room-temperature ferroelectricity at reduced dimensions. *Science* **2015**, *349*, 1314.

(13) Tang, Y.-Y.; Li, P.-F.; Shi, P.-P.; Zhang, W.-Y.; Wang, Z.-X.; You, Y.-M.; Ye, H.-Y.; Nakamura, T.; Xiong, R.-G. Visualization of Room-Temperature Ferroelectricity and Polarization Rotation in the Thin Film of Quinuclidinium Perrhenate. *Phys. Rev. Lett.* **2017**, *119*, 207602.

(14) (a) McKinnon, J. J.; Jayatilaka, D.; Spackman, M. A. Towards quantitative analysis of intermolecular interactions with Hirshfeld surfaces. *Chem. Commun.* **2007**, *37*, 3814. (b) McKinnon, J. J.; Mitchell, A. S.; Spackman, M. A. Hirshfeld surfaces: A new tool for visualising and exploring molecular crystals. *Chem. - Eur. J.* **1998**, *4*, 2136.

Table of Contents